Dynamic State Estimation Based Protection for Large-scale Renewable Energy Transmission Lines

Meng Li, Ming Nie, Jinghan He, *Fellow*, *IEEE*, and Huiyuan Zhang

***Abstract*—The development of low-carbon energy systems and renewable energy sources (RESs) are critical to solving the energy crisis around the world. However, renewable energy generation control strategies lead to fault characteristics such as fault current amplitude limitation and phase angle distortion. Focusing on large-scale renewable energy transmission lines, the sensitivity of traditional current differential protection and distance protection may be reduced, and there is even the risk of maloperation. Therefore, a suitable transmission line model is established, which considers the distributed capacitance. Afterward, a novel dynamic state estimation based protection (DSEBP) for large-scale renewable energy transmission lines is proposed. The proposed DSEBP adopts instantaneous measurements and additional protection criteria to ensure the quick action and reliability. Finally, faults are identified by checking the matching degree between the actual measurements and the established transmission line model. The performance of the proposed DSEBP is verified through PSCAD/EMTDC and real-time digital simulator (RTDS) hardware-in-loop tests. The results demonstrate that the proposed DSEBP can identify various types of faults quickly and reliably. Meanwhile, the proposed DSEBP has a better capability to withstand fault resistance and disturbance.**

***Index Terms*—Dynamic state estimation, protection, fault identification, renewable energy, transmission line, real-time digital simulator (RTDS), hardware-in-loop test.**

I. Introduction

RENEWABLE energy generation is being developed globally to reduce carbon emissions. In 2022, there are over 75 GW of wind power generation and over 190 GW of photovoltaic power generation installed worldwide [1], [2]. The new power system will be dominated by renewable energy in the future, and its rotational inertia will be greatly reduced, which will significantly reduce the ability to withstand fault shocks [3]. The operation speed of protection will be more important. However, the existing AC protection mainly relies on the power frequency phasor to identify faults [4], and the operation speed is limited by the length of window of the Fourier algorithm. Moreover, the fault characteristics of renewable energy generation are different from those of conventional power generation, and they will affect the performance of protection [5], [6]. Therefore, it is necessary to study the new method of transmission line protection using instantaneous measurements. But how to withstand the effect of distributed capacitance for instantaneous measurement protection is a big challenge.

At present, a majority of renewable energy generation plants are directly connected to the power system composed of traditional synchronous generators, and the renewable energy generation plant shows weak-infeed characteristics [7]. In the actual project, as the measured impedance is difficult to calculate accurately, the zone I distance protection on the renewable energy generation plant side is withdrawn from operation [8]. Positive-sequence impedance and negative-sequence impedance of renewable energy generation become no longer equal when a fault occurs, so there is a risk of misjudgment of protection [9]. Because of the phase angle distortion characteristic, the restrain coefficient of the traditional current differential protection may be lower than the set value, and the sensitivity decreases [10]. It is difficult for traditional protection methods to ensure rapid and reliable fault identification for large-scale renewable energy transmission lines.

For the problems of traditional protections, the existing research can be divided into two categories [11], [12]: ① performance improvements based on traditional protection methods, and ② new protection methods based on fault transient information. In [13], the proposed protection method uses the time-domain zone II distance protection as a directional discriminating element. However, the measured impedance is calculated by equating the transmission line to the *R*-*L* parameter model and ignoring the line distribution capacitance, which is only applicable to short transmission lines. In [14], the pilot protection uses the current amplitude ratio to compensate for the shortcomings of current differential protection. However, this protection method is not applicable to regions with a high proportion of renewable energy sources (RESs). The improved Euclidean distance based pilot protec-

Manuscript received: June 17, 2024; revised: October 29, 2024; accepted: November 14, 2024. Date of CrossCheck: November 14, 2024. Date of online publication: December 9, 2024.

This work was supported by National Natural Science Foundation of China-State Grid Corporation Joint Fund for Smart Grid (No. U2066210).

M. Li, M. Nie (corresponding author), and J. He are with the School of Electrical Engineering, Beijing Jiaotong University, Beijing 100044, China, and M. Nie is also with State Grid Economic and Technological Research Institute Co., Ltd., Beijing 102209, China (e-mail: mengl@bjtu.edu.cn; nieming@chinasperi.sgcc.com.cn; jhhe@bjtu.edu.cn).

H. Zhang is with China Electric Power Research Institute, State Grid Corporation of China, Beijing 100192, China (e-mail: zhanghuiyuan@epri.sgcc.com.cn).

DOI: 10.35833/MPCE.2024.000633

tion is proposed in [15], which identifies faults by calculating the Euclidean distance of the current value. But this method is still influenced by the fault characteristics of renewable energy generation.

Because of the limited performance of traditional pilot protection, researchers began to study new protection methods for fault transient characteristics. In [16], a pilot protection based on a two-port network model is proposed. This method calculates the network parameters online and compares them with the protection settings for fault identification. However, this method may be influenced by noise disturbance. Fast protection on the basis of the ratio of traveling wave energy is proposed in [17], which adds frequency information to amplify the effect of high-frequency components. However, traveling wave protection has a dead zone when the voltage is zero, and it is difficult to be applied to renewable energy transmission lines. In [18], the transient current similarity based protection is proposed, which is not influenced by the fault characteristics of renewable energy generation. However, it is also affected by distributed capacitance.

In summary, the existing protection fails to solve the problem of limited performance due to changes in the fault characteristics of renewable energy generation. Dynamic state estimation methods provide a new idea for the protection of large-scale renewable energy transmission lines [19]. In [20], the dynamic state estimation method is first applied from the field of power systems to the protection of AC transmission lines. However, the existing dynamic state estimation based protection (DSEBP) of AC transmission lines is computed in the phase domain, leading to high computational complexity. In [21], the dynamic state estimation method is used for flexible DC protection. However, it is difficult to tolerate the effects of transformer disconnection. Meanwhile, fault phase selection methods are important for the protection of high-voltage AC (HVAC) transmission lines, but none of the above protection considers fault phase selection.

A novel DSEBP for large-scale renewable energy transmission lines is proposed in this paper. Firstly, a suitable model of renewable energy transmission lines is established. Meanwhile, the distributed capacitance of the transmission line is considered. Afterward, the system measurement equations are established, and the state variables are calculated by dynamic state estimation. Finally, faults are identified by checking the matching degree between the actual measurements and the established transmission line model. The hardware-in-loop test results verify the performance of the proposed DSEBP. The key contributions of this paper are as follows.

1) The idea of dynamic state estimation is incorporated into the protection method, and the faults are identified by checking the matching degree between the transmission line and the established model. Therefore, the proposed DSEBP is not affected by interference outside the protected line, and the reliability is improved.

2) The reliability of the proposed DSEBP is improved by constructing the main and additional measurement equations. The proposed DSEBP can operate normally when the transmission line potential transformer (PT) or current transformer (CT) is disconnected.

3) The residual characteristics in the proposed DSEBP are used for fault phase selection, which does not require additional new criteria and enhances the engineering practicality.

II. Renewable Energy Transmission Line Model

A suitable model of renewable energy transmission line is the key point of the proposed DSEBP. The relationship among line length, model accuracy, and computational complexity needs to be considered.

The centralized parameter model does not consider the electromagnetic wave transmission process of the line. It has low computational complexity and is suitable for the study of low-voltage distribution networks. However, it does not consider the distributed capacitance of the line, which will cause large calculation errors when being used in long-distance transmission lines.

Frequency-dependent parameter model combines the parameter distribution and frequency-dependent characteristics and fits the line characteristic impedance and attenuation constants with reasonable rational equations. In existing transmission line models, the frequency-dependent parameter model is the most precise. However, it is more suitable for long-distance DC transmission scenarios and takes up too many computational resources.

Bergeron model is an approximate lossy transmission line model under the condition of satisfying engineering needs. Its accuracy is not so high as the frequency-dependent parameter model. However, the Bergeron model has relatively suitable computational complexity, and the AC transmission line has a fixed main frequency, which is more suitable for the study of large-scale renewable energy transmission lines. Therefore, the following analyses are based on the Bergeron model.

Mutually coupled phase voltage, current, and transmission line parameters are converted to the independent mode domain (0-1-2 modes) by the Karenbauer transformation matrix $\boldsymbol{S}$.

$$\boldsymbol{S}^{-1}=\frac{1}{3}\begin{bmatrix}1 & 1 & 1\\ 1 & -1 & 0\\ 1 & 0 & -1\end{bmatrix} \tag{1}$$

The Bergeron model of transmission line is shown in Fig. 1, where l is the length of the line; R_0 is the resistance of the line; and L_0 and C_0 are the inductance and capacitance per unit length, respectively. And subsequent analyses are indicated in the mode domain if not otherwise specified.

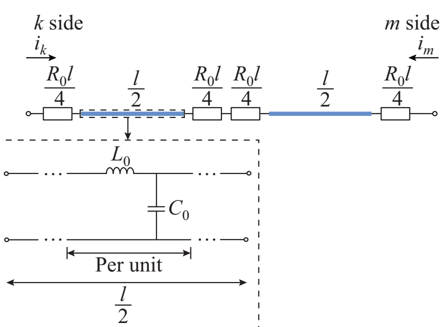

Fig. 1. Bergeron model of transmission line.

The instantaneous measurements ($i_k(t)$, $i_m(t)$, $u_k(t)$, $u_m(t)$) are used, where i and u are the voltage and current, respectively; and subscripts k and m represent the k side and m side, respectively. The model of large-scale renewable energy transmission lines based on the Bergeron model is then given as:

$$\begin{cases} i_k(t)=\dfrac{1}{Z}u_k(t)-\dfrac{1+h}{2}\left(\dfrac{1}{Z}u_m(t-\tau)+hi_m(t-\tau)\right)- \\ \qquad \dfrac{1-h}{2}\left(\dfrac{1}{Z}u_k(t-\tau)+hi_k(t-\tau)\right) \\ i_m(t)=\dfrac{1}{Z}u_m(t)-\dfrac{1+h}{2}\left[\dfrac{1}{Z}u_k(t-\tau)+hi_k(t-\tau))-\right. \\ \qquad \left.\dfrac{1-h}{2}\left(\dfrac{1}{Z}u_m(t-\tau)+hi_m(t-\tau)\right)\right] \end{cases} \tag{2}$$

where $\tau=l\sqrt{L_0C_0}$ is the traveling wave propagation time; $Z=\sqrt{L_0/C_0}+lR_0/4$; and $h=(\sqrt{L_0/C_0}-lR_0/4)/(\sqrt{L_0/C_0}+lR_0/4)$.

III. Proposed DSEBP

Faults are identified by determining whether the actual measurements match the established transmission line model. If the measurements satisfy the physical laws of the established transmission line model, the protected transmission line is healthy. On the contrary, if the protected transmission line has an internal fault, the measurements will no longer match the established transmission line model.

A. System Measurement Equation

Combined with the established transmission line model, the system measurement equation containing the measurements, state variables, and history values is established. Measurements include voltage and current values ($u_k(t)$, $u_m(t)$, $i_k(t)$, $i_m(t)$), state variables (represented by subscript v) include voltage and current values ($u_{v,k}(t)$, $u_{v,m}(t)$, $i_{v,k}(t)$, $i_{v,m}(t)$), and history values include voltage and current values before time τ ($u_k(t-\tau)$, $u_m(t-\tau)$, $i_k(t-\tau)$, $i_m(t-\tau)$, $u_{v,m}(t-\tau)$, $i_{v,m}(t-\tau)$). The system measurement equations can be established as:

$$\begin{cases} i_k(t)=\dfrac{1}{Z}u_{v,k}(t)-\dfrac{1+h}{2}\left(\dfrac{1}{Z}u_{v,m}(t-\tau)+hi_m(t-\tau)\right)- \\ \qquad \dfrac{1-h}{2}\left(\dfrac{1}{Z}u_k(t-\tau)+hi_k(t-\tau)\right) \\ i_m(t)=\dfrac{1}{Z}u_{v,m}(t)-\dfrac{1+h}{2}\left(\dfrac{1}{Z}u_k(t-\tau)+hi_k(t-\tau))\right)- \\ \qquad \dfrac{1-h}{2}\left(\dfrac{1}{Z}u_{v,m}(t-\tau)+hi_m(t-\tau)\right) \\ u_k(t)=u_{v,k}(t) \end{cases} \Rightarrow$$

$$\boldsymbol{z}_{\text{main}}(t)=f(\boldsymbol{x}_{\text{main}}(t),t)=\boldsymbol{H}_{\text{main}}\boldsymbol{x}_{\text{main}}(t)+\boldsymbol{C}_{\text{main}}(t) \tag{3}$$

$$\begin{cases} u_k(t)=Zi_{v,k}(t)+\dfrac{1+h}{2}(u_m(t-\tau)+Zhi_{v,m}(t-\tau))+ \\ \qquad \dfrac{1-h}{2}(u_k(t-\tau)+Zhi_k(t-\tau)) \\ u_m(t)=Zi_{v,m}(t)+\dfrac{1+h}{2}(u_k(t-\tau)+Zhi_k(t-\tau))+ \\ \qquad \dfrac{1-h}{2}(u_m(t-\tau)+Zhi_{v,m}(t-\tau)) \\ i_k(t)=i_{v,k}(t) \end{cases} \Rightarrow$$

$$\boldsymbol{z}_{\text{add}}(t)=f(\boldsymbol{x}_{\text{add}}(t),t)=\boldsymbol{H}_{\text{add}}\boldsymbol{x}_{\text{add}}(t)+\boldsymbol{C}_{\text{add}}(t) \tag{4}$$

where $\boldsymbol{z}(t)$ is the column vector of measurements; $\boldsymbol{x}(t)$ is the column vector of state variables; $\boldsymbol{H}$ is a Jacobian matrix; $\boldsymbol{C}(t)$ is the column vector of history values; f is a function that incorporates $\boldsymbol{x}(t)$ and t; and subscripts main and add represent the main and additional measurement equations, respectively. By combining the main equation (3) with the additional equation (4), the dependability of the protection is improved.

B. Protection Algorithm

The idea of dynamic state estimation is incorporated into the protection by determining if the actual measurements can match the established transmission line model. The specific implementation method is weighted least squares.

$$\min J=(\boldsymbol{z}(t)-f(\boldsymbol{x}(t),t))^{\mathrm{T}}\boldsymbol{W}(\boldsymbol{z}(t)-f(\boldsymbol{x}(t),t))=\boldsymbol{r}(t)^{\mathrm{T}}\boldsymbol{W}\boldsymbol{r}(t) \tag{5}$$

where $\boldsymbol{W}=diag\{1/\sigma_1^2, 1/\sigma_2^2, ..., 1/\sigma_{num}^2\}$ is the weight matrix, σ is the standard deviation, and num is the number of measurements.

When line parameters are known, $f(\boldsymbol{x}(t),t)$ is a linear function and the Jacobi matrix is a constant matrix. Therefore, the optimal estimated state variables are obtained:

$$\hat{\boldsymbol{x}}(t)=(\boldsymbol{H}^{\mathrm{T}}\boldsymbol{W}\boldsymbol{H})^{-1}\boldsymbol{H}^{\mathrm{T}}\boldsymbol{W}(\boldsymbol{z}(t)-\boldsymbol{C}(t)) \tag{6}$$

The estimated measurements $\hat{\boldsymbol{z}}(t)$ and the sum of the square of the normalized residuals ζ can be calculated as:

$$\hat{\boldsymbol{z}}(t)=h(\hat{\boldsymbol{x}}(t),t)=\boldsymbol{H}\hat{\boldsymbol{x}}(t)+\boldsymbol{C}(t) \tag{7}$$

$$\boldsymbol{r}(t)=\hat{\boldsymbol{z}}(t)-\boldsymbol{z}(t) \tag{8}$$

$$\zeta=\sum_{i=1}^{num}\left(\frac{\hat{\boldsymbol{z}}_i(t)-\boldsymbol{z}_i(t)}{\sigma_i}\right)^2 \tag{9}$$

where $\boldsymbol{r}(t)$ is the residual of measurements.

C. Criteria of Proposed DSEBP

The deviation between actual and estimated measurements is defined as the residual $\boldsymbol{r}$. And ζ can be applied to identify whether an internal fault occurs.

If no internal fault occurs, the measurements match the established transmission line model and ζ satisfies the chi-square distribution $\chi^2(K)$. However, if an internal fault occurs, the measurements will no longer match the established transmission line model, and ζ does not meet the chi-square distribution. Therefore, ζ can be employed to determine whether the line is healthy.

The degree of freedom F indicates the redundancy of the system measurement equation. And $P(F)$ is the confidence level, indicating the probability of the goodness of fit:

$$P(F)=1-P[\zeta\geq\chi_\gamma^2(F)]=1-\int_{\chi_\gamma^2}^{\infty}f(\chi^2)\mathrm{d}\chi^2 \tag{10}$$

where $P[\zeta\geq\chi_\gamma^2(F)]$ is the probability of chi-square distribution given $\zeta\geq\chi_\gamma^2(F)$ with F degrees of freedom; and γ is the probability that $\chi^2(F)$ is larger than the threshold $\chi_\gamma^2(F)$.

According to (10), if $P(F)$ is low, it indicates that the measurements do not match the established transmission line model and ζ does not meet the chi-square distribution. Therefore, an internal fault occurs. On the contrary, if $P(F)$ is high, it indicates that the transmission line is healthy.

The main and additional protection criteria are included in the protection criterion to enhance reliability. The protection issues the trip signal $Trip(t)$ when ζ satisfies the criterion.

$$Trip_{\text{main}}(t)=\begin{cases}1 & \int_{t-T_{\text{set}}}^{t} S_{\text{main}}(\tau)\mathrm{d}\tau \geq T_{\text{delay}} \\ 0 & \int_{t-T_{\text{set}}}^{t} S_{\text{main}}(\tau)\mathrm{d}\tau < T_{\text{delay}}\end{cases} \tag{11a}$$

$$S_{\text{main}}(t)=\begin{cases}1 & \zeta_{\text{main}} \geq \chi_{\alpha}^{2}(F) \\ 0 & \zeta_{\text{main}} < \chi_{\alpha}^{2}(F)\end{cases} \tag{11b}$$

$$Trip_{\text{add}}(t)=\begin{cases}1 & \int_{t-T_{\text{set}}}^{t} S_{\text{add}}(\tau)\mathrm{d}\tau \geq T_{\text{delay}} \\ 0 & \int_{t-T_{\text{set}}}^{t} S_{\text{add}}(\tau)\mathrm{d}\tau < T_{\text{delay}}\end{cases} \tag{12a}$$

$$S_{\text{add}}(t)=\begin{cases}1 & \zeta_{\text{add}} \geq \chi_{\alpha}^{2}(F) \\ 0 & \zeta_{\text{add}} < \chi_{\alpha}^{2}(F)\end{cases} \tag{12b}$$

$$Trip_{\text{ope}}(t)=\begin{cases}1 & Trip_{\text{main}}(t)=1 \wedge Trip_{\text{add}}(t)=1 \\ 0 & \text{else}\end{cases} \tag{13}$$

where $\chi_{\alpha}^{2}(F)$ is the threshold for ζ; and T_{delay} is a user-defined trip delay. Equations (11) and (12) are the main and additional protection criteria, respectively, and $Trip_{\text{ope}}(t)$ means that the relay sends a trip signal.

In this paper, $\chi_{\gamma}^{2}(F)$ is set to be 6.63. When ζ is greater than 6.63, it is known that there is 99% probability that an internal fault occurs on the protected line by consulting the chi-square distribution table. However, it does not indicate that there is 1% probability of protection misoperation, because the protection criterion contains a user-defined trip delay. When ζ remains larger than $\chi_{\gamma}^{2}(F)$ for the trip delay, the protection relay will issue the trip signal. Combining the reliability and sensitivity of the proposed DSEBP, the reset time T_{set} is set to be 2 ms, the trip delay T_{delay} is set to be 5, and the standard deviation of measurements is set to be 0.02 p.u..

D. Protection Method Implementation

AC transmission line protection device with the voltage level of 220 kV and above needs to be equipped with a fault phase selection function. If the single-phase-to-ground fault happens, the fault phase should be selected properly. Meanwhile, the single-phase circuit breaker needs to be tripped. But if the phase-to-phase fault (AB), phase-to-phase-to-ground fault (AB-G), or three-phase fault occurs, the three-phase circuit breaker needs to be tripped. Therefore, an accurate and effective method of fault phase selection is particularly important. The proposed DSEBP in this paper has a natural fault phase selection function and does not require additional criteria.

From the above analyses, the measurements are converted to the mode domain by Karenbauer transformation. The 0-mode component contains the measurement information of the three phases, the 1-mode component contains the measurement information of A-B two phases, and the 2-mode component contains the measurement information of A-C two phases.

When an internal single-line-to-ground (A-G) fault occurs on the protected transmission line, the fault component of phase A is decomposed into 1-mode, 2-mode, and 0-mode by the Karenbauer transformation, which will result in a larger residual for all three modes. But B-phase and C-phase are in normal operation, which does not lead to a larger residual.

Therefore, when an internal A-G fault occurs on the protected transmission line, the residuals of 1-, 2-, and 0-modes maintain almost the same value of growth. Similarly, when an internal B-G fault occurs on the protected transmission line, the residuals of 1-mode and 0-mode maintain almost the same value of growth, while the residuals of 2-mode do not increase. When an internal C-G fault occurs on the protected transmission line, the residuals of 2-mode and 0-mode maintain almost the same value of growth, while the residuals of 1-mode do not increase. Therefore, the fault phase selection criteria are shown in (14)-(16), respectively.

$$\begin{cases}\varepsilon_{low} \leq \dfrac{\zeta_1}{\zeta_0} \leq \varepsilon_{up} \\ \varepsilon_{low} \leq \dfrac{\zeta_2}{\zeta_0} \leq \varepsilon_{up}\end{cases} \tag{14}$$

$$\begin{cases}\varepsilon_{low} \leq \dfrac{\zeta_1}{\zeta_0} \leq \varepsilon_{up} \\ \dfrac{\zeta_2}{\zeta_0} \leq \varepsilon_{sp}\end{cases} \tag{15}$$

$$\begin{cases}\dfrac{\zeta_1}{\zeta_0} \leq \varepsilon_{sp} \\ \varepsilon_{low} \leq \dfrac{\zeta_2}{\zeta_0} \leq \varepsilon_{up}\end{cases} \tag{16}$$

where ζ_1, ζ_2, and ζ_0 are the sums of the square of the normalized residuals of 1-, 2-, and 0-modes, respectively; and the limits ε_{up}, ε_{low}, and ε_{sp} are set to be 1.5, 0.5, and 0.01, respectively, by combining model accuracy and measurement error.

As can be observed from the above equations, when ζ meets (14), (15), or (16), it means an internal A-G, B-G, or C-G fault occurs, respectively. If ζ does not meet the above equations, the three-phase circuit breaker is tripped. The flowchart of the proposed DSEBP is shown in Fig. 2.

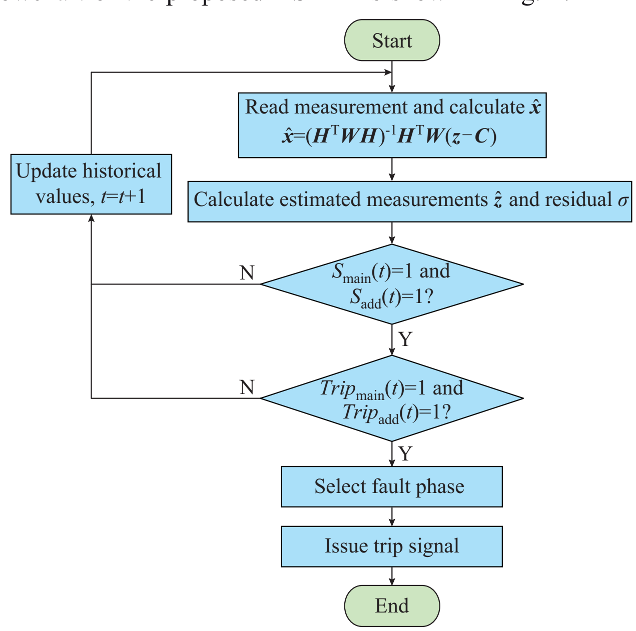

Fig. 2. Flowchart of proposed DSEBP.

IV. Analysis of Influencing Factors

A. Fault Resistance and Distributed Capacitance

The proposed DSEBP is based on comparing the matching degree between actual measurements and the established transmission line model to identify faults. Therefore, even if internal faults occur on the protected transmission line with high fault resistance, the physical laws of the actual transmission line will change fundamentally, and the actual measurements will not match the established transmission model. Theoretically, the proposed DSEBP can withstand high fault resistance.

The Bergeron model established in Section III considers the transmission characteristics of the traveling wave, which incorporates the effect of the distributed capacitance of transmission lines. Therefore, the proposed DSEBP will not be affected by the distributed capacitance of transmission line.

B. Noise Disturbance

Affected by the electromagnetic radiation of the power equipment in the power system, there must be a noise signal in the transmission line. Therefore, when there is a noise signal in the measurement, the main factor affecting the protection performance is the magnitude of the noise. Under normal operating conditions, noise disturbance will cause increase in residuals. But ζ that is much smaller than the threshold does not affect the performance of the proposed DSEBP.

C. PT/CT Disconnection

The proposed DSEBP utilizes additional equations to enhance the reliability and eliminate the effect of disconnected transformers on the pilot protection.

As shown in (3), the measurements do not include the voltage measurement value on the *m* side. Therefore, the dynamic state estimation results on the *k* side are not affected when the PT on the *m* side of the line is disconnected. Similarly, as shown in (4), the measurements do not include the current measurement value on the *m* side. And the dynamic state estimation results on the *k* side are not affected when the line CT on the *m* side is disconnected.

In combination with the protection criteria, the protection device is only allowed to issue a trip signal if both the main and additional criteria are satisfied. Therefore, considering the dynamic state estimation results of (3) and (4) together, the proposed DSEBP can still operate normally when the transformer is disconnected.

D. Protection Operation Time

The protection operation time mainly consists of: ① fault propagation time, ② optical fiber communication time, ③ protection start-up time, ④ calculation time of protection algorithm, and ⑤ delay of relay contact action.

Fault propagation time includes the time taken for the fault traveling wave to propagate from the fault point to the installation point of protection device when the fault occurs.

For optical fiber communication time, theoretically, signals are transmitted in optical fiber at 200 km/ms. Meanwhile, the protection algorithm needs sampling values from both sides of the line.

For the calculation time of the protection algorithm, the fastest time that can be known by the protection criterion is 1 ms. Section V considers only the calculation time of the protection algorithm.

For protection start-up time and delay of the relay contact action, comprehensive consideration is given in Section VI.

E. Fault Characteristic of Renewable Energy Generation

There is a fundamental difference in fault characteristics between traditional synchronous power generation and renewable energy generation. However, the proposed DSEBP focuses on the physical laws of the established transmission line model itself. In other words, it can be understood as decoupling the protected line from an external system. If an internal fault happens, the physical laws of the actual transmission line will be broken, and proposed DSEBP will issue the trip signal quickly and reliably. Therefore, the proposed DSEBP is not affected by fault characteristics and control strategies of RESs.

V. Simulation and Analysis

The large-scale renewable energy transmission system shown in Fig. 3 is constructed by PSCAD/EMTDC. The renewable energy power plant is a full-power inverter station, whose rated capacity is 450 MW. The main parameters are shown in Table AI of Appendix A.

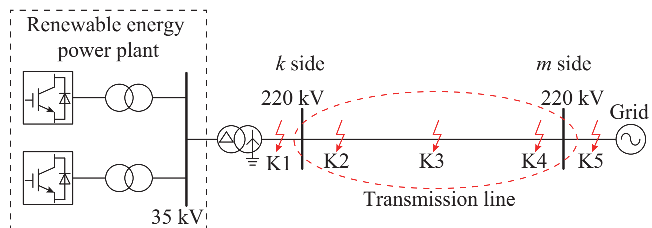

Fig. 3. Large-scale renewable energy transmission system.

A. Accuracy of Established Transmission Line Model

In order to verify the accuracy of the established transmission line model, the PSCAD simulation results are taken into the dynamic state estimation algorithm for calculation. The accuracy of the established transmission line model is verified by comparing the error between the measurements and the estimated value. The comparison results are shown in Fig. 4.

As can be observed in Fig. 4, the measurements are consistent with the estimated value, and the relative error is less than 1%. The established transmission line model can calculate the current and voltage values accurately. Therefore, the established transmission line model is accurate.

B. Performance of Various Fault Locations and Types

According to Fig. 3, the fault locations are set as K1-K5, where K1 and K5 are located on the outside of the bus on the *k* side (renewable energy generation plant side) and the bus on the *m* side (grid side). The other three fault points K2-K4 are set to be 0%, 50%, and 100% of the transmission line from the bus on the *k* side. Various types of faults are simulated to verify the performance of the proposed DSEBP, including A-G, BC, BC-G, and ABC faults.

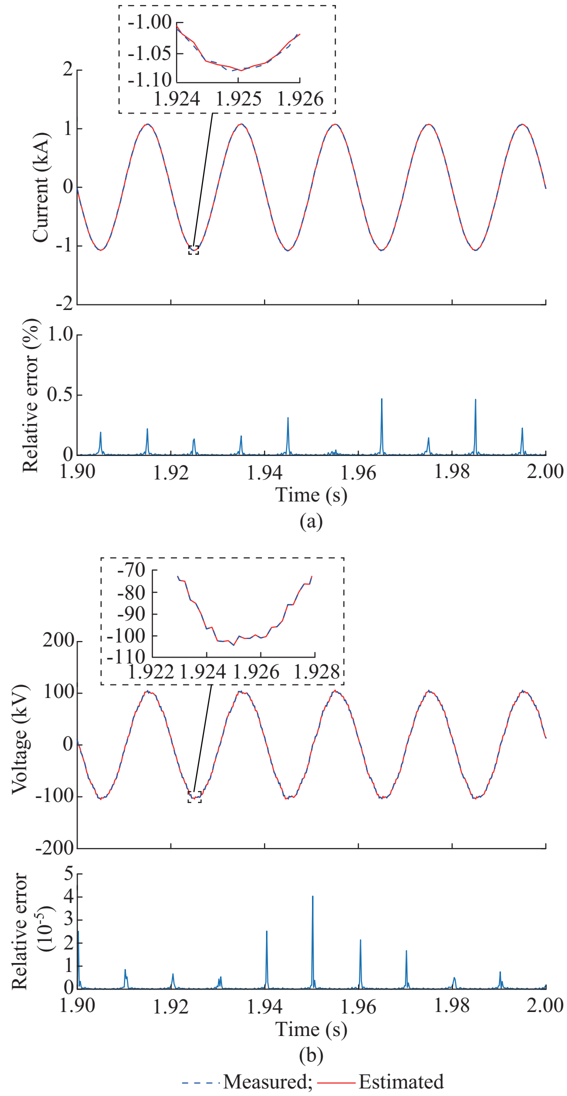

Fig. 4. Comparison results of measured and estimated values. (a) Current and relative error. (b) Voltage and relative error.

The simulation results at different fault locations are shown in Fig. 5. In Fig. 5(a), before an internal fault occurs, the estimated current wave is consistent with the measured current wave, and ζ is nearly zero. However, there are remarkable differences between the estimated and measured current waves during the internal fault. Referring to the criterion and fault phase selection criterion of the proposed DSEBP, ζ exceeds $\chi_{\gamma}^{2}(F)$ and meets the protection criterion. Therefore, the proposed DSEBP sends out the trip signal correctly.

In Fig. 5(b), the estimated current wave is consistent with the measured current wave before an external fault occurs. During the external fault, the estimated and measured current waves remain consistent. According to the logic of the proposed DSEBP, ζ is much less than $\chi_{\gamma}^{2}(F)$. And the proposed DSEBP can correctly identify the external fault and will not misoperate.

The performance of the proposed DSEBP under different fault locations and fault types is shown in Table I. It shows that the proposed DSEBP can quickly identify internal faults and will not misoperate when an external fault occurs.

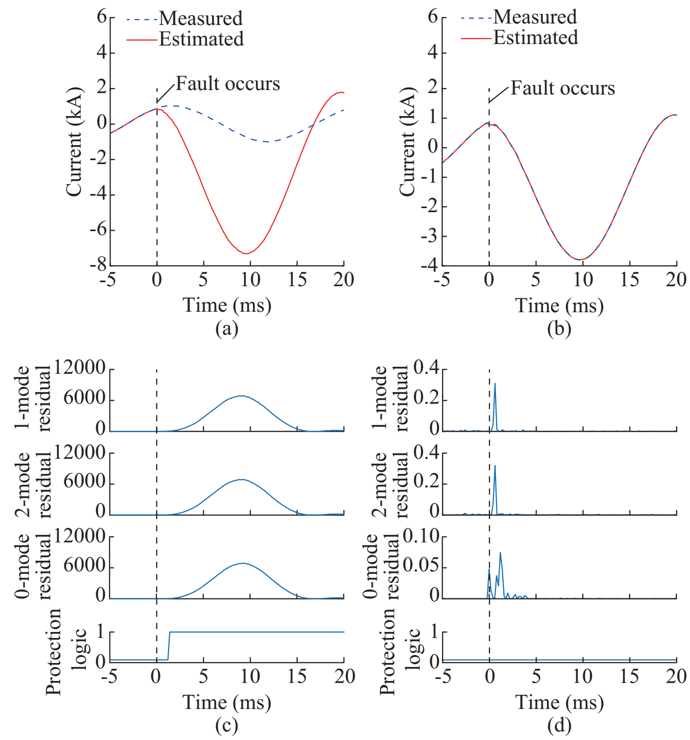

Fig. 5. Simulation results at different fault locations. (a) Current under A-G fault at K3. (b) Current under A-G fault at K1. (c) Residuals under A-G fault at K3. (d) Residuals under A-G fault at K1.

TABLE I
PERFORMANCE OF PROPOSED DSEBP UNDER DIFFERENT FAULT LOCATIONS AND FAULT TYPES

Fault location	Fault type	Behavior of protection	
		k side	*m* side
K1	A-G		
	BC		
	BC-G		
	ABC		
K2	A-G	1.2 ms, trip A	1.2 ms, trip A
	BC	1.0 ms, trip ABC	1.4 ms, trip ABC
	BC-G	1.0 ms, trip ABC	1.2 ms, trip ABC
	ABC	1.0 ms, trip ABC	1.2 ms, trip ABC
K3	A-G	1.4 ms, trip A	1.4 ms, trip A
	BC	1.0 ms, trip ABC	1.0 ms, trip ABC
	BC-G	1.0 ms, trip ABC	1.0 ms, trip ABC
	ABC	1.0 ms, trip ABC	1.0 ms, trip ABC
K4	A-G	1.4 ms, trip A	1.4 ms, trip A
	BC	1.2 ms, trip ABC	1.0 ms, trip ABC
	BC-G	1.2 ms, trip ABC	1.0 ms, trip ABC
	ABC	1.2 ms, trip ABC	1.0 ms, trip ABC
K5	A-G		
	BC		
	BC-G		
	ABC		

C. *Performance Influenced by Fault Resistance*

To test the performance of the proposed DSEBP under different fault resistances, internal faults with different fault types are set. The simulation results are shown in Table II. It shows that the proposed DSEBP can identify internal faults with 200 Ω fault resistance sensitively and rapidly.

TABLE II
SIMULATION RESULTS UNDER DIFFERENT FAULT TYPES

Fault location	Fault type	Behavior of protection	
		k side	*m* side
K2	A-G, 200 Ω	1.8 ms, trip A	1.8 ms, trip A
	BC, 200 Ω	1.4 ms, trip ABC	1.6 ms, trip ABC
	BC-G, 200 Ω	1.6 ms, trip ABC	1.8 ms, trip ABC
	ABC, 200 Ω	1.0 ms, trip ABC	1.2 ms, trip ABC
K3	A-G, 200 Ω	2.0 ms, trip A	2.0 ms, trip A
	BC, 200 Ω	1.0 ms, trip ABC	1.0 ms, trip ABC
	BC-G, 200 Ω	1.2 ms, trip ABC	1.2 ms, trip ABC
	ABC, 200 Ω	1.0 ms, trip ABC	1.0 ms, trip ABC
K4	A-G, 200 Ω	2.0 ms, trip A	2.0 ms, trip A
	BC, 200 Ω	1.2 ms, trip ABC	1.0 ms, trip ABC
	BC-G, 200 Ω	1.4 ms, trip ABC	1.2 ms, trip ABC
	ABC, 200 Ω	1.2 ms, trip ABC	1.0 ms, trip ABC

D. Performance Influenced by Noise Disturbance

The capability of the proposed DSEBP affected by noise disturbance is also tested. The 25 dB noise is added to measurement data to verify the protection performance. As shown in Fig. 6, for the A-G fault at K1, the simulation result is given.

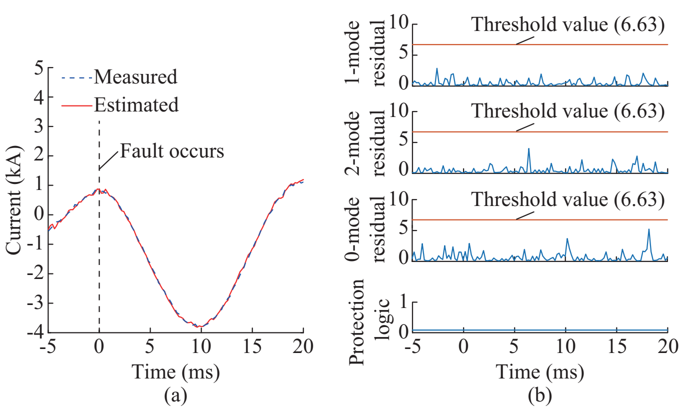

Fig. 6. Simulation results for protection performance influenced by noise disturbance. (a) Current. (b) Residuals.

The estimated and measured current wave remains basically the same trend before and during the external fault. Meanwhile, the measured current becomes unsmooth due to noise disturbance. According to the protection logic, ζ is much less than $\chi_{\gamma}^{2}(F)$, and the proposed DSEBP will not misoperate under the 25 dB noise disturbance.

E. Performance Influenced by Transformer Disconnection

To verify the capability of the proposed DSEBP to withstand transformer disconnection, the PT of phase A and CT on *k* side are disconnected at 2.5 s and the A-G fault at K3 occurs at 3 s.

In Fig. 7(a) and (c), the estimated current on *m* side in the main criterion remains the same as the measured current before the fault occurs. Although the additional protection criterion is affected by the PT disconnection when the fault occurs, the main criterion is not affected by the PT disconnection. Therefore, the PT disconnection does not influence the proposed DSEBP to identify the fault accurately.

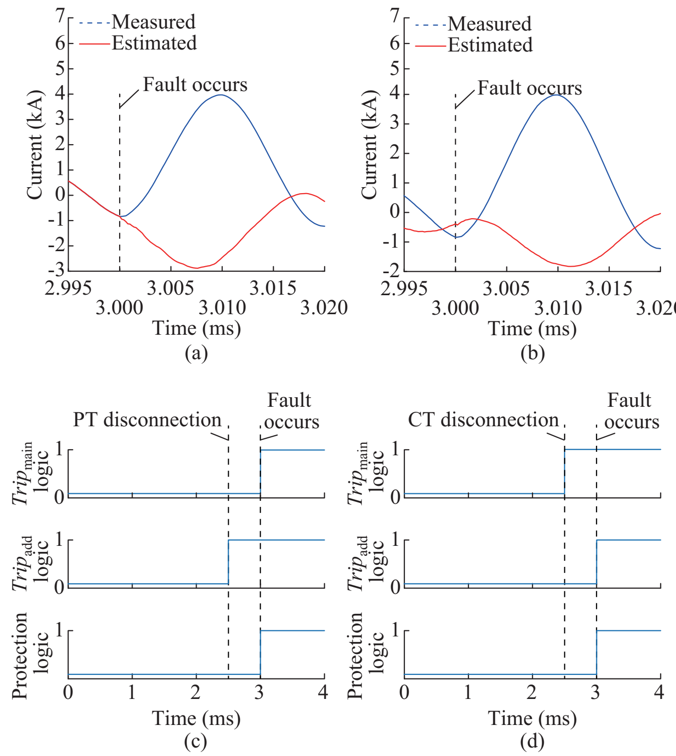

Fig. 7. Simulation results for protection performance influenced by disconnection. (a) Current under PT disconnection. (b) Current under CT disconnection. (c) Logics under PT disconnection. (d) Logics under CT disconnection.

In Fig. 7(b) and (d), the estimated current on *m* side in the main criterion presents a large deviation from the measured current because of the influence of the CT disconnection on *k* side. Although the main protection criterion is affected by the CT disconnection, the additional criterion is not affected by the CT disconnection. Therefore, the CT disconnection does not influence the proposed DSEBP to identify the fault accurately.

F. Performance Influenced by Synchronization Error

For double-ended protection methods, the synchronization error might affect the correct fault identification. As shown in Fig. 8, the 200 μs synchronization error is added to the A-G fault at K1, and the simulation results are obtained.

Due to the synchronization error, there are some deviations between the estimated and measured current waves when the external fault occurs. However, the trend and amplitude of the current wave remain consistent. Meanwhile, ζ is much less than $\chi_{\gamma}^{2}(F)$, and the proposed DSEBP will not misoperate.

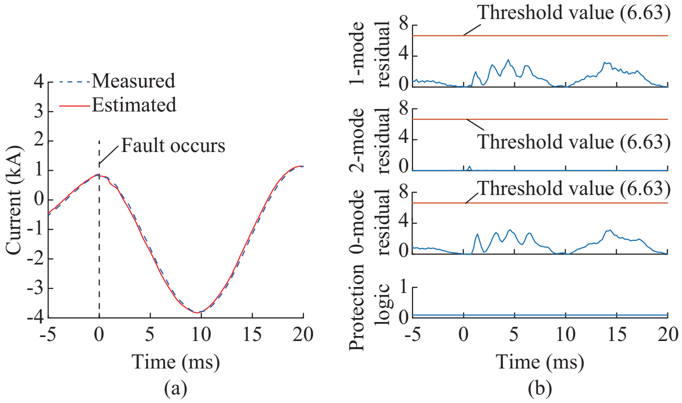

Fig. 8. Simulation results for performance influenced by synchronization error. (a) Current. (b) Residuals.

G. Performance Influenced by Lightning Interference

To verify the ability of the proposed DSEBP to withstand lightning interference, the standard lightning wave (1.2/50 μs) is used to simulate the healthy line. Lightning interference happens at 0 ms, and the simulation results are shown in Fig. 9.

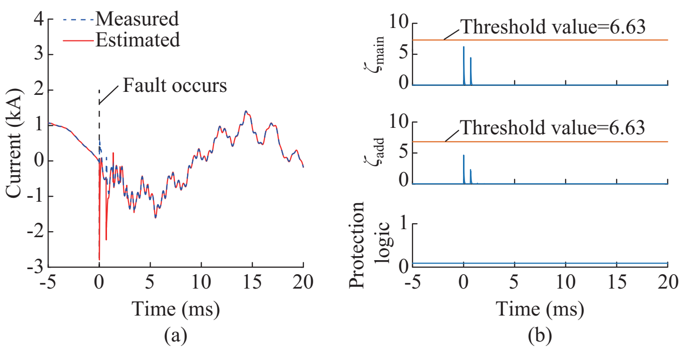

Fig. 9. Simulation results for protection performance influenced by lightning interference. (a) Current. (b) Residuals.

Before the lightning interference occurs, ζ is nearly zero. When it occurs, ζ increases rapidly but is much less than $\chi^2_\gamma(F)$. According to the protection logic, the proposed DSEBP can ignore the lightning interference correctly.

H. Comparison Between Traditional Current Differential Protection (TCDP), Traditional Phase Comparison Protection (TPCP), and Proposed DSEBP

In order to compare the performances of TCDP, TPCP, and the proposed DSEBP, the BC-G fault with fault resistances of 0.01 Ω and 200 Ω occurs at K3. The corresponding comparison results are given in Fig. 10.

In Fig. 10(a) and (b), when the BC-G fault occurs, the TCDP identifies the internal fault correctly. But if the BC-G fault with fault resistance of 200 Ω occurs, the TCDP cannot identify it, and the restrain coefficients of B and C phases are lower than the TCDP set value. The sensitivity of TCDP decreases. In Fig. 10(c) and (d), when the BC-G fault with fault resistance of 200 Ω occurs, the phase difference between B and C phases on both sides of the line is lower than the TPCP set value. And the TPCP cannot accurately identify the internal fault.

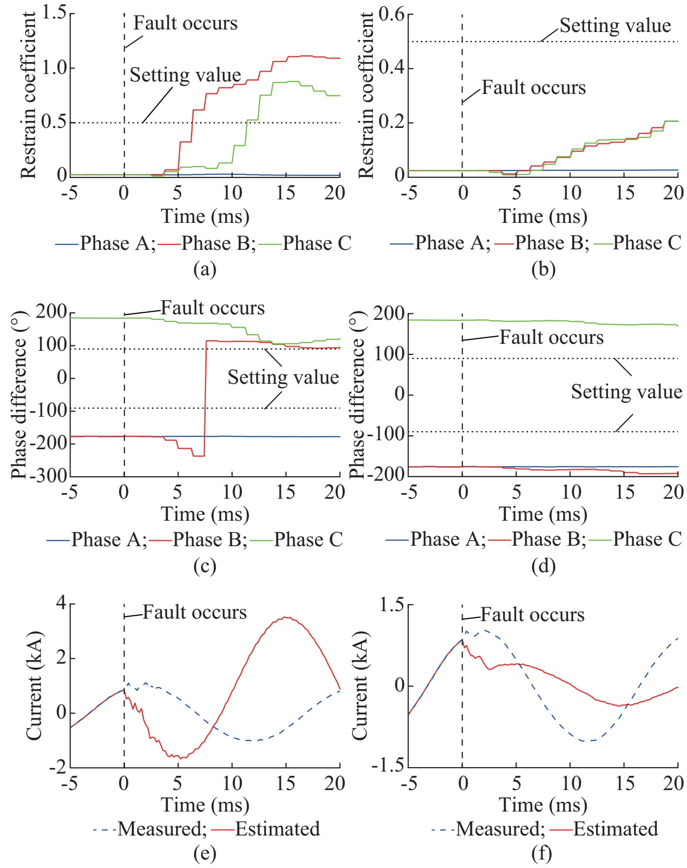

Fig. 10. Comparison results. (a) Restrain coefficient with fault resistance of 0.01 Ω using TCDP. (b) Restrain coefficient with fault resistance of 200 Ω using TCDP. (c) Phase difference with fault resistance of 0.01 Ω using TPCP. (d) Phase difference with fault resistance of 200 Ω using TPCP. (e) Current with fault resistance of 0.01 Ω using proposed DSEBP. (f) Current with fault resistance of 200 Ω using proposed DSEBP.

In Fig. 10(e) and (f), the estimated current wave is consistent with the measurement before an internal fault occurs. However, the estimated and measured current waves show significant differences when the internal fault occurs. Based on the criterion and fault phase selection criterion of the proposed DSEBP, ζ exceeds $\chi^2_\gamma(F)$ and satisfies the protection algorithm. Therefore, the trip signal is issued correctly.

VI. Hardware-in-Loop Experimental Validation

In order to verify the performance of the proposed DSEBP, the relevant experiments are carried out in a real-time digital simulator (RTDS) hardware-in-loop test system. Unlike traditional offline simulation software, it can embed the protection algorithms and control strategies into the hardware so that the performance of protection prototype in real environments can be tested.

As shown in Fig. 11, the experimental platform is built, and the proposed DSEBP is implemented by the protection prototype device. The sending side employs the renewable energy generation plant, and the receiving side employs the traditional AC system. The rated capacity of the renewable energy generation plant is 100 MW. The rated voltage and the length of the protected line are 220 kV and 30 km, respectively.

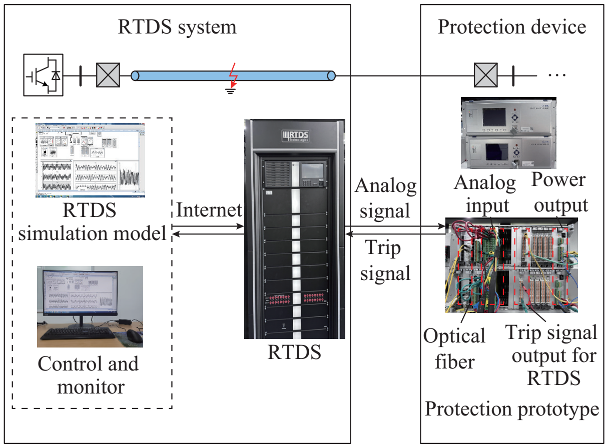

Fig. 11. RTDS hardware-in-loop test system.

The RTDS hardware-in-loop simulation results under the internal A-G fault at K3, internal ABC-G fault at K3, and external A-G fault at K5 (outside of the renewable energy generation plant side) are shown in Fig. 12. In Fig. 12(a) and (d), significant differences between the estimated and measured current waves during the internal fault, and the protection prototype device issues a trip signal correctly. In Fig. 12(c), before and during the external fault, the trend of the estimated and measured current waves remain basically consistent. The protection prototype device will not misoperate.

The RTDS hardware-in-loop test indicates that the performance of proposed DSEBP is consistent with the simulations. Meanwhile, the trip signals of the protection prototype device show that the proposed DSEBP can identify the fault correctly and quickly, which is applicable to large-scale renewable energy transmission lines.

At the same time, the RTDS hardware-in-loop test results of the proposed DSEBP are listed in Table III, with a good fault identification performance. Under different types of faults, the protection prototype can operate within 13 ms.

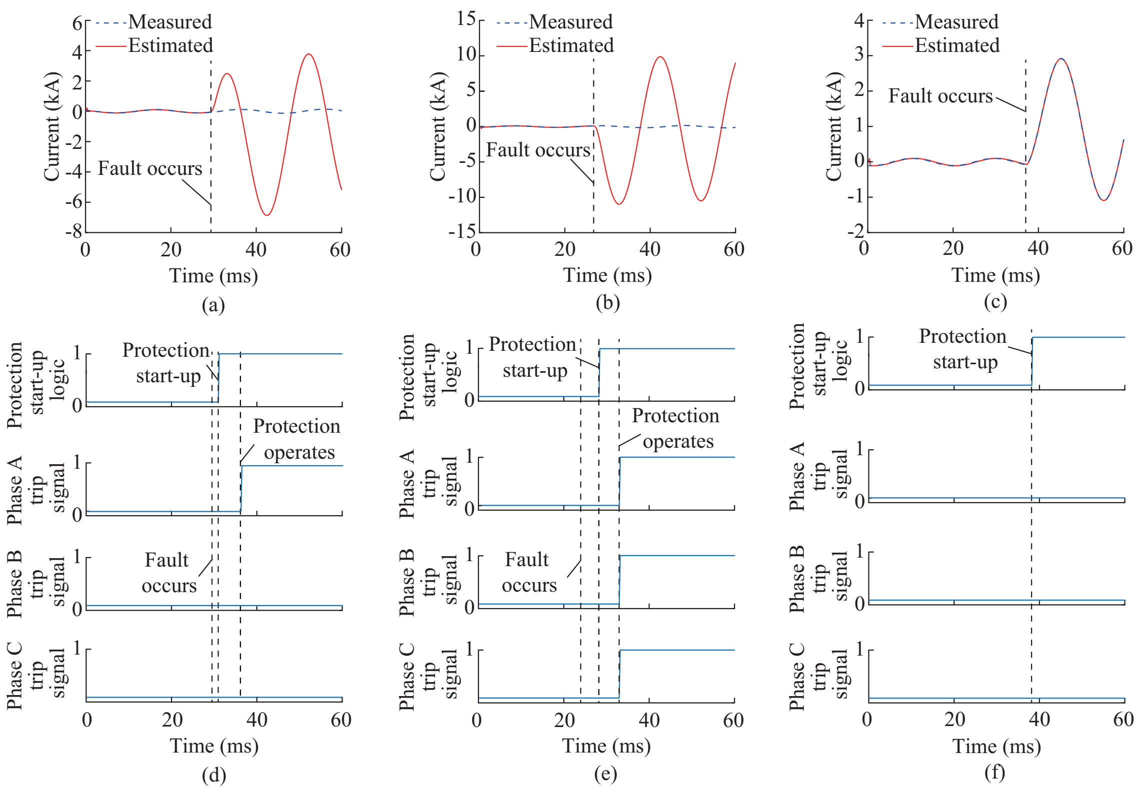

Fig. 12. RTDS hardware-in-loop test results. (a) Current under A-G fault at K3. (b) Current under ABC-G fault at K3. (c) Current under A-G fault at K5. (d) Trip logics under A-G fault at K3. (e) Trip logics under ABC-G fault at K3. (f) Trip logics under A-G fault at K5.

VII. Conclusion

Renewable energy generation control strategies lead to the decrease of sensitivity of traditional protection methods. Therefore, a novel DSEBP for large-scale renewable energy transmission lines is proposed in this paper. Simulation results and RTDS hardware-in-loop test results verify the feasibility of the proposed DSEBP. Conclusions are as follows.

1) The proposed DSEBP focuses on the physical laws of the established transmission line model, which decouples the protected line from the external system. In other words, the renewable energy generation control strategies will not affect the proposed DSEBP, and the reliability will be improved.

2) The proposed DSEBP can select the fault phase using the residual characteristics of dynamic state estimation without additional criteria, which facilitates engineering applications.

3) The proposed DSEBP can operate within 2 ms (calculation time of the protection algorithm) when internal faults occur, and can operate normally with fault resistance of 200 Ω. In addition, it has high reliability to withstand 25 dB noise disturbance and 200 μs synchronization error. Meanwhile, it utilizes redundant measurements and additional equations to eliminate the effects of transformer disconnection.

TABLE III
RTDS Hardware-in-loop Test Results of Proposed DSEBP

Fault location	Fault type	Behavior of protection	
		k side	*m* side
K1	A-G		
	BC		
	BC-G		
	ABC		
K2	A-G	11.6 ms, trip A	11.4 ms, trip A
	BC	11.6 ms, trip ABC	11.2 ms, trip ABC
	BC-G	12 ms, trip ABC	11.2 ms, trip ABC
	ABC	12.8 ms, trip ABC	11.8 ms, trip ABC
K3	A-G	10.8 ms, trip A	12.8 ms, trip A
	BC	10.6 ms, trip ABC	11.2 ms, trip ABC
	BC-G	12.6 ms, trip ABC	12 ms, trip ABC
	ABC	10 ms, trip ABC	12 ms, trip ABC
K4	A-G	11 ms, trip A	11.6 ms, trip A
	BC	11 ms, trip ABC	12.8 ms, trip ABC
	BC-G	12.2 ms, trip ABC	12.4 ms, trip ABC
	ABC	11.6 ms, trip ABC	11 ms, trip ABC
K5	A-G		
	BC		
	BC-G		
	ABC		

Appendix A

TABLE AI
Main Parameters of Simulation Model

Model	Parameter	Value
Transmission line	Rated voltage	220 kV
	Length of transmission line	100 km
	Sampling frequency	5 kHz
Full-power inverter station	Number of units	90
	Sigle unit capacity	5 MW
	Rated voltage and frequency	0.69 kV, 50 Hz
	Proportional and integral constants of current loop	25, 0.01
	Proportional and integral constants of voltage loop	0.5, 0.02

References

[1] P. Mishra, A. K. Pradhan, and P. Bajpai, "Adaptive distance relaying for distribution lines connecting inverter-interfaced solar PV plant," *IEEE Transactions on Industrial Electronics*, vol. 68, no. 3, pp. 2300-2309, Mar. 2021.

[2] L. Zheng, K. Jia, W. Wu *et al*., "Cosine similarity based line protection for large scale wind farms Part II – the industrial application," *IEEE Transactions on Industrial Electronics*, vol. 69, no. 3, pp. 2599-2609, Mar. 2022.

[3] M. M. Shabestary and Y. A. I. Mohamed, "Asymmetrical ride-through and grid support in converter-interfaced DG units under unbalanced conditions," *IEEE Transactions on Industrial Electronics*, vol. 66, no. 2, pp. 1130-1141, Feb. 2019.

[4] K. A. Saleh, M. S. El Moursi, and H. H. Zeineldin, "A new protection scheme considering fault ride through requirements for transmission level interconnected wind parks," *IEEE Transactions on Industrial Informatics*, vol. 11, no. 6, pp. 1324-1333, Dec. 2015.

[5] J. Zhang, B. Zhang, and C. Wang, "Improved schemes for conventional current-based phase selectors in wind power systems," *IET Generation, Transmission & Distribution*, vol. 12, no. 21, pp. 5781-5788, Nov. 2018.

[6] Z. Hu, B. Li, Y. Zheng *et al*., "Fast distance protection scheme for wind farm transmission lines considering *R-L* and Bergeron models" *Journal of Modern Power Systems and Clean Energy*, vol. 11, no. 3, pp. 840-852, May 2023.

[7] T. G. Bolandi, H. Seyedi, S. M. Hashemi *et al*., "Impedance-differential protection: a new approach to transmission-line pilot protection," *IEEE Transactions on Power Delivery*, vol. 30, no. 6, pp. 2510-2518, Dec. 2015.

[8] Y. Liang, W. Li, and Y. Huo, "Zone I distance relaying scheme of lines connected to MMC-HVDC stations during asymmetrical faults: problems, challenges, and solutions," *IEEE Transactions on Power Delivery*, vol. 36, no. 5, pp. 2929-2941, Oct. 2021.

[9] K. Jia, Z. Yang, Y. Fang *et al*., "Influence of inverter-interfaced renewable energy generators on directional relay and an improved scheme," *IEEE Transactions on Power Electronics*, vol. 34, no. 12, pp. 11843-11855, Dec. 2019.

[10] L. Zheng, K. Jia, B. Yang *et al*., "Singular value decomposition based pilot protection for transmission lines with converters on both ends," *IEEE Transactions on Power Delivery*, vol. 37, no. 4, pp. 2728-2737, Aug. 2022.

[11] C. Chao, X. Zheng, Y. Weng *et al*., "Adaptive distance protection based on the analytical model of additional impedance for inverter-interfaced renewable power plants during asymmetrical faults," *IEEE Transactions on Power Delivery*, vol. 37, no. 5, pp. 3823-3834, Oct. 2022.

[12] Y. Liang, W. Li, and Z. Lu, "Effect of inverter-interfaced renewable energy power plants on negative-sequence directional relays and a solution," *IEEE Transactions on Power Delivery*, vol. 36, no. 2, pp. 554-565, Apr. 2021.

[13] C. Wang, S. Sun, X. Mao *et al*., "Longitudinal direction protection of time domain distance applicable to the outgoing line of a double-fed wind farm," *Power System Protection and Control*, vol. 49, no. 13, pp. 82-94, Jul. 2021.

[14] K. Jia, Z. Yang, Z. Zhu *et al*., "Pilot protection based on current amplitude ratio for teed line in inverter-interfaced renewable energy power plants," *Electric Power Automation Equipment*, vol. 39, no. 12, pp. 82-88, Dec. 2019.

[15] Z. Yang, W. Liao, H. Wang *et al*., "Improved Euclidean distance based pilot protection for lines with renewable energy sources," *IEEE Transactions on Industrial Informatics*, vol. 18, no. 12, pp. 8551-8562, Dec. 2022.

[16] S. Liu, L. Zhang, C. Fu *et al*., "A new two-port network model-based pilot protection for AC transmission lines," *IEEE Transactions on Power Delivery*, vol. 35, no. 2, pp. 473-482, Apr. 2020.

[17] S. Gao, X. Song, H. Ye *et al*., "Transient energy protection based on wavelet packet transform for hybrid bipolar HVDC transmission system," *IET Generation, Transmission & Distribution*, vol. 15, no. 12, pp. 1775-1786, Feb. 2021.

[18] K. Jia, Y. Li, Y. Fang *et al*., "Transient current similarity based protection for wind farm transmission lines," *Applied Energy*, vol. 225, pp. 42-51, Sept. 2018.

[19] A. P. S. Meliopoulos, G. J. Cokkinides, P. Myrda *et al*., "Dynamic state estimation-based protection: status and promise," *IEEE Transactions on Power Delivery*, vol. 32, no. 1, pp. 320-330, Feb. 2017.

[20] Y. Liu, A. P. S. Meliopoulos, R. Fan *et al*., "Dynamic state estimation based protection on series compensated transmission lines," *IEEE Transactions on Power Delivery*, vol. 32, no. 5, pp. 2199-2209, Oct. 2017.

[21] B. Wang, Y. Liu, D. Lu *et al*., "MMC-HVDC transmission line protection based on Bergeron model and state estimation," in *Proceedings of 2019 8th Renewable Power Generation Conference (RPG)*, Shanghai, China, Oct. 2019, pp. 1-6.

Meng Li received the B.S. and Ph.D. degrees in electrical engineering from North China Electric Power University, Beijing, China, in 2007 and 2018, respectively. He is currently an Associate Professor at the School of Electrical Engineering, Beijing Jiaotong University, Beijing, China. His research interest includes AC/DC grid protection.

Ming Nie received the Ph.D. degree in electrical engineering from Beijing Jiaotong University, Beijing, China, in 2024. His research interests include AC/DC grid protection and control.

Jinghan He received the M.Sc. degree in electrical engineering from Tianjin University, Tianjin, China, in 1994, and the Ph.D. degree in electrical engineering from Beijing Jiaotong University, Beijing, China, in 2007. She has been a Professor with the School of Electrical Engineering, Beijing Jiaotong University, since 2000. She is a Fellow of IEEE and currently serving as Chairman of IEEE PES China Membership Committee. Her research interests include power system relay protection, and monitoring and protection of railway traction power supply systems.

Huiyuan Zhang received the Ph. D. degree in electrical engineering from Beijing Jiaotong University, Beijing, China, in 2023. Her research interests include electrical engineering, high-voltage engineering, partial discharge, and sensor.